Section 7

Global and regional climate models, sensitivity and impact experiments, response to external forcing

Increasing carbon and nitrogen stocks in active layer under permafrost thawing

M.M. Arzhanov
A.M. Obukhov Institute of Atmospheric Physics RAS,
3 Pyzhevsky Lane, 119017 Moscow, Russia
arzhanov@ifaran.ru

Ongoing and projected warming is most pronounced in the northern high latitudes. It can result in changes in the thermal and hydrological conditions of permafrost, seasonal dynamics and spatial distribution of plant communities in ecosystems and initiate natural processes with negative consequences for infrastructure of settled territories. The total increase of the mean permafrost temperature and thickness of the thawed layer above permafrost can cause extensive settlement of the ground surface and activate some destructive geocriological processes. Soils in the high latitudes are expected to respond strongly to climate change, but still little is known about associated carbon and nitrogen variability. Thawing of permafrost soils and increase of active layer thickness can intensify a decay of the organic matter and lead to an increase of greenhouse gases emission from soil to the atmosphere that, in turn, reinforces the global warming. These processes can essentially change dynamics of carbon and nitrogen fluxes in ecosystems of the polar regions.

Main characteristics of permafrost using numerical scheme of heat and moisture transfer in the atmosphere-underlying surface-soil accounting for dynamics of frozen and thaw layers boundaries with water phase changes [1] are obtained. External atmospheric forcing for this scheme is given for the period of 2001-2100 according to realized the SRES A1B scenario using the climate models ensemble from the WCRP CMIP3 Multi-Model Database. By the late 21st century, the increase in annual mean air temperature reaches 5-6ºC in the high latitudes of Western Siberia and Chukotka (Fig. 1a).

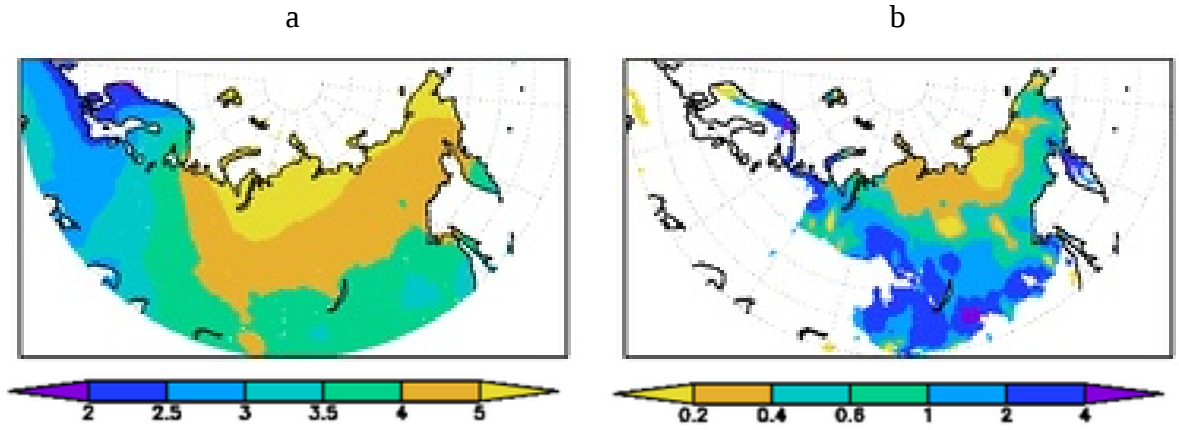

Figure 1. Change in annual mean air temperature, ºC (a) and thaw depth, m (b) of Northern Eurasia for 2091-2100 relative to 2001-2010.

The annual warming by 2100 equals 3-5 ºC in Eastern Siberia and 2-3ºC in Nothern Europe. In winter, the spatial structure of the air temperature is similar to annual mean changes, but with strongly warming reaching 6 ºC in the Western Siberia. The warming is generally larger in winter than in summer.

For this climate scenario, depths of seasonal thaw and taliks in regions occupied by permafrost in 21st century are calculated. Maximal changes (3-4 m) of melted layer depth due to talik formation are expected at the southern boundary of Eurasian permafrost in the end of the 21st century (Fig. 1b). According to be obtained estimates, these changes amount to 2-3

m in the northern part of the Western Siberia and in the Baikal region, while they are expected about 0.2-0.3 m in the northern part of the Eastern Siberia. During the last 20 to 30 years of observations the increases in talik thickness range from 0.2 to 6.7 m in all geocryological zones of the northern European Russia [2].

Increase of melted layer depth may involve carbon and nitrogen stored in the permafrost in the global biogeochemical cycle. The soil carbon and nitrogen concentration distribution are taken from ORNL DAAC data set [3]. According to the model calculations, the carbon concentrations will increase substantially and exceed 6-8 kg/m2 in the southern permafrost region by 2100 (Fig. 2a). This scenario is also valid for nitrogen concentration (Fig. 2b).

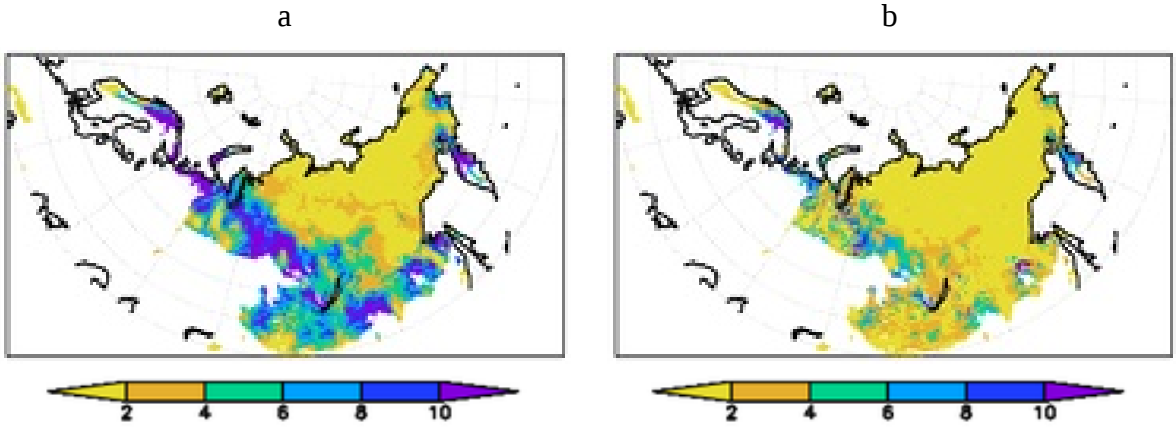

Figure 2. Change of the carbon (a) and nitrogen (b) concentrations (kg/m^2) in frozen soils of Northern Eurasia for 2091-2100 relative to 2001-2010 by thawing.

Carbon and nitrogen storage in the active layer of the northern Euroasian permafrost in the beginning of the 21st century is estimated to be 89 GtC and 41 GtN respectively. Increase of the carbon storage due to the permafrost melt is estimated to be about 60%. Soil carbon changes under the process of edoma thaw are estimated to be 5.4 GtC to the end of the 21st century while the nitrogen increase can amount to 25 GtN. These results compare well with the estimates by [4].

Acknowledgements
The World Climate Research Program's (WCRP) Coupled Model Intercomparison Project phase 3 (CMIP3) Multi-Model Database, NATO Collaborative Linkage Grant, The Russian Fondation for Basic Research, The program of the Earth Sciences Department of the Russian Academy of Sciences

References

[1] Arzhanov M. M., Eliseev A. V., Demchenko P. F., Mokhov I. I., and Khon V. Ch. Simulation of Thermal and Hydrological Regimes of Siberian River Watersheds under Permafrost Conditions from Reanalysis Data // Izvestiya, Atmospheric and Oceanic Physics, 2008, Vol. 44, No. 1, pp. 83–89.
[2] Oberman N. Contemporary permafrost degradation of European North of Russia // In Proceedings of the Ninth International Conference on Permafrost, June 29 — July 3. Fairbanks, Alaska. 2008. Vol. 2. P. 1305-1310.
[3] Oak Ridge National Laboratory Distributed Active Archive Center (ORNL DAAC). 2009. SAFARI 2000 Web Page. Available online [http://daac.ornl.gov/S2K/safari.html] from ORNL DAAC, Oak Ridge, Tennessee, U.S.A. Accessed November 5, 2009.
[4] Schuur E.A.G., Bockheim J., Canadell J.G. et al. Vulnerability of Permafrost Carbon to Climate Change: Implications for the Global Carbon Cycle // BioScience. 2008. V. 58. № 8. P. 701-714.

Permafrost modelling with CLASS and CRCM/CLASS

J.-P. Blanchette[1], L. Sushama[1], R. Laprise [1], M. Allard[2], R. Harvey[3]

[1]Centre pour l'étude et la simulation à l'échelle régionale, Université du Québec à Montréal, Montréal, Canada, email: jpblanc@sca.uqam.sca; [2]Centre d'Études Nordiques, Université Laval, Québec, Canada; [3]Canadian Centre for Climate Modelling and Analysis (CCCMa), Environment Canada

INTRODUCTION

Recent studies by Alexeev et al. (2007) and Nicolsky et al. (2007) have shown that using shallow soil models with zero flux bottom boundary conditions to study near-surface permafrost and its evolution in future climate can give inaccurate assessments. Their offline study with deep and shallow soil model configurations suggests that near-surface permafrost degradation occurs at an accelerated rate in shallow configurations compared to deep configurations. However, Lawrence et al. (2008) using offline simulations with the Community Climate Model showed that the global area covered by near-surface permafrost converged to practically the same amount at the end of the 21st century for deep and shallow configurations. Many initiatives are underway in different climate modelling groups to better represent near-surface permafrost in climate models. Selected results based on offline simulations performed with the latest version of the Canadian LAnd Surface Scheme (CLASS; Verseghy, 1991, Verseghy et al., 1993) looking at the thermal and hydrologic regimes of permafrost regions are presented in this paper. CLASS is highly suited for permafrost studies due to its very flexible soil configuration, both in terms of the depth of the soil model and the thickness of soil layers. CLASS is also the land surface scheme used in the fifth generation of the Canadian Regional Climate Model (CRCM5; Zandra et al., 2008). Some results based on CRCM5/CLASS, with different configurations of CLASS, are also discussed in this paper.

RESULTS

Results from CLASS offline simulations, driven by CRCM outputs, for the 1961–2100 period suggest that the use of a deeper soil configuration (i.e., 100 m deep with a total of 20 layers) compared to a shallow configuration (i.e., 4.1 m with 3 or 10 layers), as well as organic matter instead of mineral soil when appropriate, delays permafrost degradation by adding thermal inertia to the soil.

Figure 1a shows CLASS simulated temperatures for deep and shallow configurations, which suggest warmer (cooler) temperatures in summer and fall (winter and spring) for the shallow configuration. Overall, the evolution of the soil temperature difference suggests that the shallow configuration accumulates more energy from year to year, which translates into a greater temperature difference over time. The offline simulations, however, do not capture the land-atmosphere feedback and currently efforts are underway to study soil thermal and moisture regimes in permafrost underlain regions using CRCM5 with interactive permafrost (i.e., CRCM5 with the deeper version of CLASS for the LSS). Preliminary results with CRCM5/CLASS current climate simulations (1975-2002) also suggest similar results as obtained with the offline CLASS simulations. Figures. 1b and 1c show the difference in the CRCM5/CLASS simulated temperature for the first 10 cm of soil and at 4.1 m, respectively, for the deep vs. shallow configurations for the month of November, which suggests higher temperatures simulated with CRCM5 with the shallow CLASS configuration. However, the soil temperature differences in these coupled simulations are larger than those obtained with the offline simulations of CLASS and could be partly due to the soil-atmosphere feedbacks, as suggested by the fact that the difference in air temperature difference for the two configurations is positively correlated with the soil temperature difference of the first layer. Important differences in other surface fields (snow cover, albedo, runoff, etc) have also been noticed for the CRCM5/CLASS simulations with different configurations. The most important is snow cover, with onset of snow and snow-melt occurring during the periods when the maximum difference in soil temperature between the two configurations is noted.

CONCLUSIONS

Important differences in the soil thermal and moisture regimes are noted for shallow and deep soil model configurations in the offline CLASS and coupled CRCM5/CLASS simulations. The use of a shallow soil model, especially with a zero flux bottom boundary condition, as used in many climate models, can lead to unrealistic energy distribution and can affect the quality of model simulated soil thermal and moisture regimes. It is hoped that the coupled CRCM5/CLASS with deep soil configuration will provide better estimates of permafrost evolution when applied to future climate.

ACKNOWLEDGEMENTS

This work was supported by the Alexander Graham Bell Canada Graduate Scholarship CGS D from NSERC (Canada) and by the Réal-Décoste Scholarship from Ouranos and FQRNT (Québec).

REFERENCE

Alexeev VA, Nicolsky DJ, Romanovsky VE, Lawrence DM. 2007. An evaluation of deep soil configurations in the CLM3 for improved representation of permafrost. *Geophysical Research Letter* **34**: L09502

Lawrence DM, Slater AG, Romanovsky VE, Nicolsky DJ. 2008. Sensitivity of a model projection of near-surface

permafrost degradation to soil column depth and representation of soil organic matter. *J. Geophys. Res.* **113**: F02011.

Nicolsky DJ, Romanovsky VE, Alexeev VA, Lawrence DM. 2007. Improved modeling of permafrost dynamics in a GCM land-surface scheme. *Geophysical Research Letter* **34**: L08501.

Verseghy DL. 1991. CLASS – A Canadian land surface scheme for GCMS, I. Soil model and coupled runs. *International Journal of Climatology* **11**: 111-133.

Verseghy DL, McFarlane NA, Lazare M. 1993. CLASS – A Canadian land surface scheme for GCMS, II. Vegetation model and coupled runs. *International Journal of Climatology* **13**: 347-370.

Zandra, A., Caya, D., Côté, J., Dugas, B., Jones, C.,Laprise, R., Winger, K., & Caron, L.-P. 2008. The Next Canadian Regional Climate Model, *Physics in Canada*, **64**(2): 75-83.

(a)

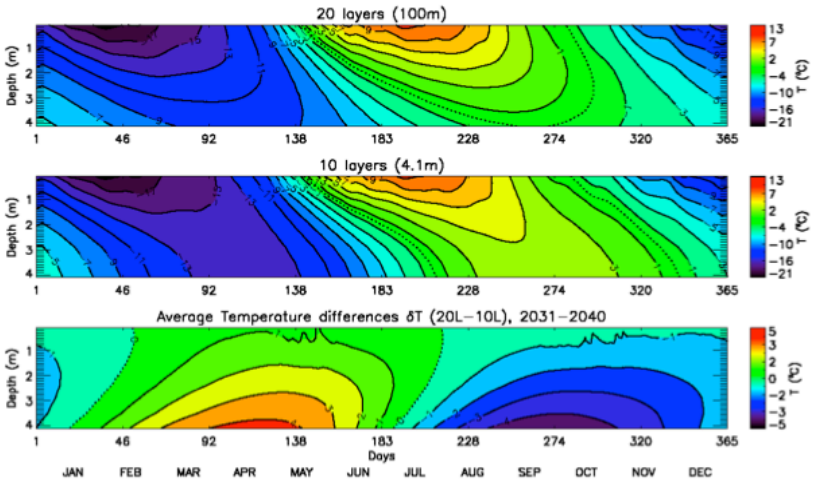

(b) (c)

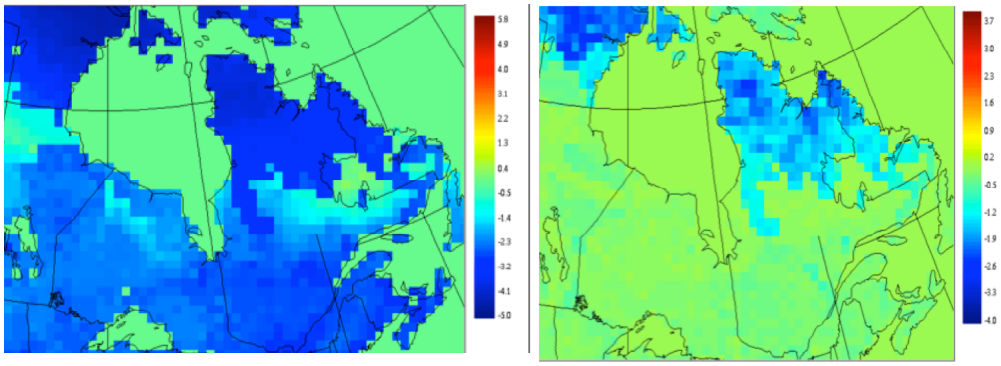

Figure 1. a) Ten-year (2031-2040) mean annual cycle of soil temperature for the first 4.1m, for the deep (top panel; 100 m deep with 20 layers) and shallow (middle panel; 4.1 m deep with 10 layers) soil model configurations, and their differences (bottom panel) from the offline simulations. Dashed lines correspond to 0°C isotherm. b) Difference in the CRCM5/CLASS simulated first soil layer (10 cm) temperature, for the month of November, for the deep and shallow configurations; The deep configuration is up to around 2°C cooler at this time of the year, compared to 0.5°C with offline simulations. c) as in b), but at 4.1m with differences as high as 5°C.

Comparison of two methods to implement rivers in Oceanic General Circulation Models

Martial Boutet, Flavien Gouillon, Rémy Baraille, Yves Morel
SHOM
martial.boutet@shom.fr

Building on the work of *Schiller et al.* (2010), this study investigates the impact of two usual methods to implement rivers on the dynamics of the river plume. We perform numerical simulations using the HYbrid Coordinate Ocean Model (hereafter HYCOM) from the NRL (HYCOM-NRL) and the SHOM (HYCOM-SHOM). The main difference between the two experiments presented below is associated with the implementation of rivers. Indeed, the HYCOM-NRL represents the river as a salinity flux (salinity relaxation) and thus does not consider the river debit. The HYCOM-SHOM represents the river as a true mass flux at the boundary (true barotropic river inflow). We expect that adding the velocity terms will change the river plume structure and the local dynamics.

Model configuration

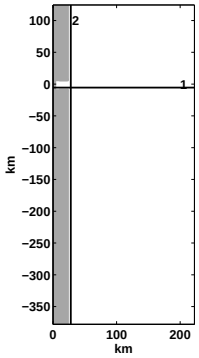

Figure 1: Schematic of the model configuration. Black lines show locations of vertical sections.

We used an idealized coastal basin configuration similar to *Schiller et al.* (2010) (200 km in the across-shore direction and 500 km in the along-shore direction with a model grid resolution of 2.5 km) and an estuary (20 km long and 15 km wide). Depth is uniform and set to 20 m (Figure 1). The initial condition is a barotropic ocean (28°C and 35 PSU) at rest. The vertical mixing scheme used is the K-Profile Parametrization (KPP) and a no-slip condition is imposed at the lateral boundaries. **In the HYCOM-SHOM, the river debit is a freshwater inflow (0 PSU) at 28°C while the HYCOM-NRL uses a salinity relaxation.** For further details, the reader is referred to the flat control experiment in *Schiller et al.* (2010).

Results

Snapshots of surface salinity and surface currents fields are presented below for both configurations at day 60 :

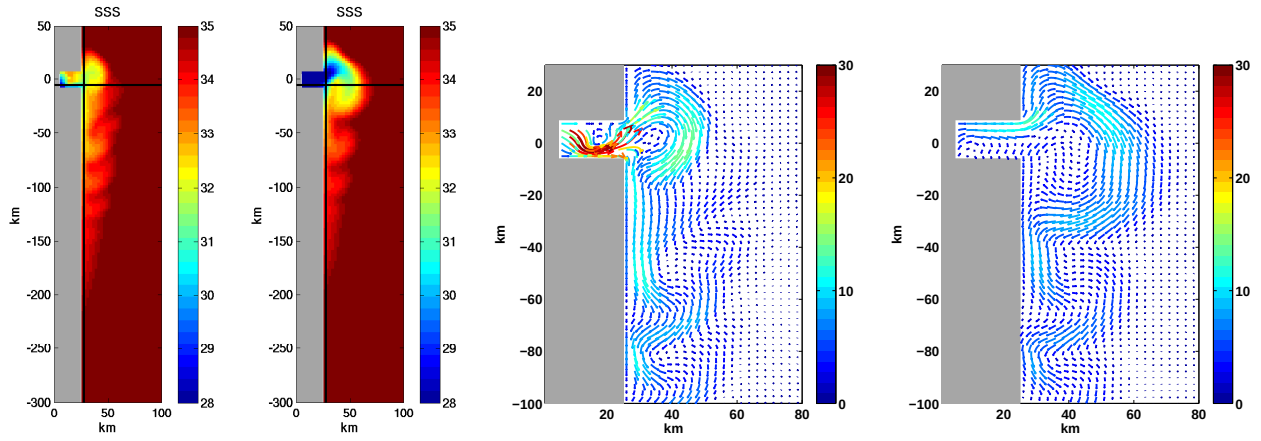

Figure 2: Sea Surface Salinity (PSU) (left panels) and surface velocities in cm.s^{-1} (right panels) for the HYCOM-SHOM and the HYCOM-NRL.

For both simulations, we observe the development of a recirculating bulge and a coastal current flowing southward. Barotropic and baroclinic instabilities develop along this current and the southward extension is more important in the HYCOM-SHOM. Visual inspection of Figure 2 clearly shows that there are different dynamics caused by the introduction of momentum inside the estuary. Indeed, for

the HYCOM-SHOM, there is a recirculating zone inside the estuary associated with higher velocities. Furthermore, the estuary dynamics impacts the shape of the plume and velocities inside the bulge. The velocities for the HYCOM-SHOM are stronger but the size of the bulge is smaller. This could be explained by more mixing induced by more shear.

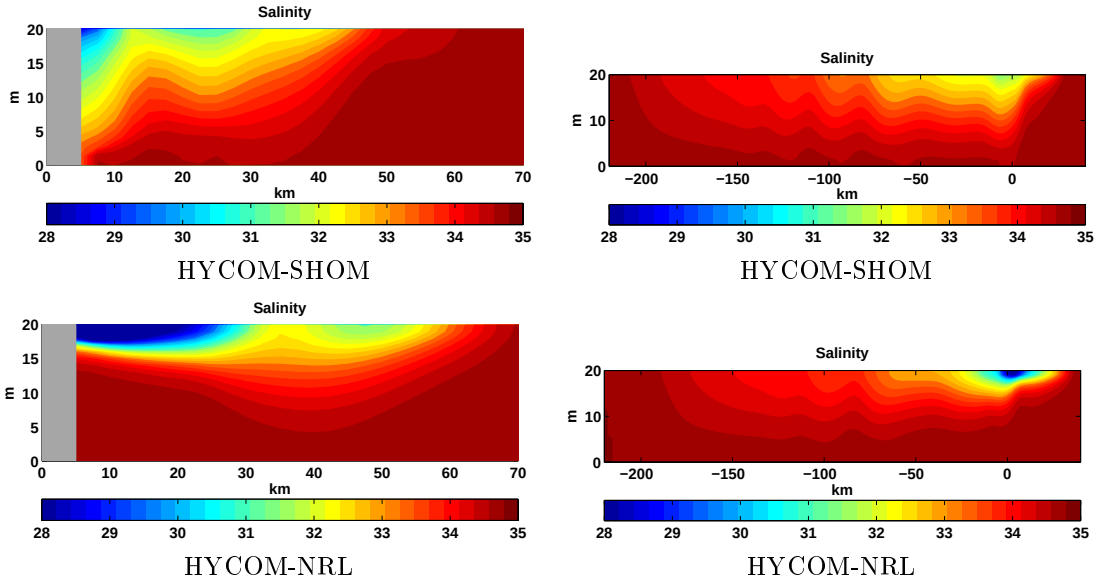

Figure 3: Across-shore salinity (PSU) vertical sections along section 1 (the estuary mouth is located at 25 km) (left panels) and along-shore salinity (PSU) vertical sections along section 2.

It is clear that the vertical mixing is different in both configurations (Figure 3). Indeed, in the HYCOM-SHOM, waters in the estuary and inside the bulge are fresher than for the HYCOM-NRL in which there is a quasi-two-layered flow. The buoyancy circulation has also a more important vertical extension in the HYCOM-SHOM.

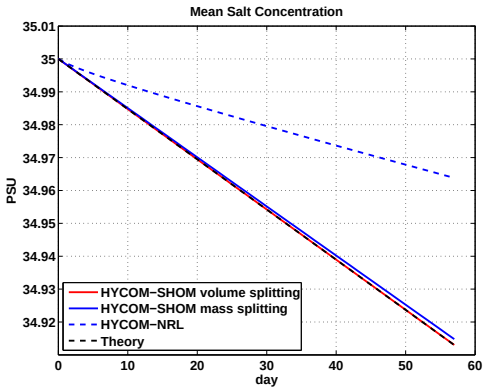

Figure 4: Time evolution of the volume integrated salinity for the HYCOM-SHOM and the HYCOM-NRL.

It is important to note that since the river representation is not the same (mass flux *vs.* relaxation), the volume integrated salinity is not similar. To correct this inconsistency, values of the river debit in the HYCOM-SHOM are changed in order to have the same freshwater introduced volume in the domain. The time evolution of the volume integrated salinity before debit correction is shown in Figure 4. In the HYCOM-SHOM, we prescribed a debit of 1000 $m^3.s^{-1}$ and theoretical evolution is computed assuming an introduction of $8.64x10^7$ m^3 of freshwater per day. The volume splitting calculation uses volume conservation while mass splitting calculation uses mass conservation. The HYCOM-NRL uses only mass splitting and we use volume splitting for HYCOM-SHOM simulations which gives more accurate results when compared to the analytical solution.

Conclusion

The structure and the shape of the river bulge and of the coastal current are highly influenced by the local dynamics in the estuary which is mainly controlled by how the river is represented. The HYCOM-SHOM uses a more physically consistent representation of the river as it includes the momentum. Future studies including other forcing terms such effect of atmospheric pressure, winds and tides are planned in order to study storm surges within the estuary.

References

Schiller, R., Kourafalou, V., 2010. Modeling river plume dynamics with the HYbrid Coordinate Ocean Model.Ocean Modelling 33, 101-117

Assessment of methane release from hydrates in oceanic sediments due to possible climate changes in the 21st century.

S.N. Denisov, M.M. Arzhanov, A.V. Eliseev, I.I. Mokhov

A.M. Obukhov Institute of Atmospheric Physics RAS, Moscow, Russia
denisov@ifaran.ru

Methane hydrates, ice-like compounds in which methane is held in crystalline cages formed by water molecules, are widespread in areas of permafrost and along continental margins (i.e, at intermediate water depths, from 250 m to several thousand meters water depth), where they are stabilized by in situ pressure and temperature fields. The widely used "consensus" global estimate of hydrate-bound methane carbon is ~ 10000 GtC (~ $20*10^{15}$ m^3 of methane) [1]. For comparison, the global inventory of fossil fuels including coal is estimated to be around 5000 GtC [2], which is in the same order of magnitude.

Massive releases of methane from hydrates have been mentioned to be responsible for rapid climate changes in the past. The Paleocene/Eocene thermal maximum is an example of a transient period with drastic climate change most likely caused by a release of 1500-2000 Gt of methane carbon within a several thousand years [3].

There is some concern, that the expected global warming may lead to hydrate instability in future and thus to an enhanced emission of methane. Accordingly, it is important to quantify the possible methane release and its impact on climate system.

In present work we tried to assess possible methane release from hydrates in the 21st century. Methane hydrate formation assumed to occur upon appropriate temperature and hydrostatic pressure conditions which are set correspondingly to [4]. Temperature profile of sediments is simulated using the model of heat and moisture transport in soil [5] adapted for oceanic conditions. Ocean bottom temperature simulations from the GFDL and INM climate models under SRES-A2 anthropogenic scenario for the 21st century are used as an upper boundary conditions. Geothermal flux of 50 mW/m^2 is set on the lower boundary. Hydrates are supposed to saturate 5% of pore space in hydrate stability zone (HSZ) [6].

Estimated total methane release in 21st century (Fig. 1) equals to ~ $10.2*10^{13}$ m^3 (~ 60 GtC) for GFDL climate model forcing and ~ $6.2*10^{13}$ m^3 (~ 35 GtC) for INM model. It corresponds to average emissions of 600 MtC/yr and 350 MtC/yr on the ocean bottom accordingly. Simulated hydrate dissociation occurs mostly in high latitudes. These estimates are close to total anthropogenic and natural emissions of methane to atmosphere of ~ 500 MtC/yr [7] but the bulk of this methane is oxidized by microbes in the water column [8].

This work was supported by the Russian Foundation for Basic Research, the programs of Russian Academy of Sciences and Russian Ministry of Education and Science.

References

[1] Kvenvolden K.A. Methane hydrate – a major reservoir of carbon in the shallow geosphere? *Chemical Geology,* 1988, 71, 41-51.

[2] Rogner H.H. An assessment of world hydrocarbon resources. *Annu. Rev. Energy Environ.,* 1997, 22, 217-62

[3] Dickens G.R., O'Neil J.R., Rea D.K. and Owen R.M. Dissociation of oceanic methane hydrate as a cause of the carbon isotope excursion at the end of Paleocene. *Paleoceanography,* 1995, 10, 965-971.
[4] Reagan M.T., Moridis G.J. Dynamic response of oceanic hydrate deposits to ocean temperature change. *J. Geophys. Res.*, 2008, 113, C12023.
[5] Arzhanov M.M., Eliseev A.V., Demchenko P.F., Mokhov I.I., and Khon V.Ch. Simulation of thermal and hydrological regimes of Siberian river watersheds under permafrost conditions from reanalysis data. *Izvestiya, Atmos. Oceanic Phys., 2008, 44 (1), 83-89.*
[6] Holbrook W.S., Hoskins H., Wood W.T., Stephen R.A., Lizaralde D. and Leg 164 Science Party. Methane hydrate and free gas on the Blake Ridge from vertical seismic profiling. *Science* 1996, 273, 1840-1843.
[7] Lelieveld J., Crutzen P.J., Dentener F.J. Changing concentration, lifetime and climate forcing of atmospheric methane. *Tellus,* 1998, 50B (2), 128-150.
[8] Reeburgh W.S. Oceanic Methane Biogeochemistry. *Chem. Rev.,* 2007, 107, 486-513.

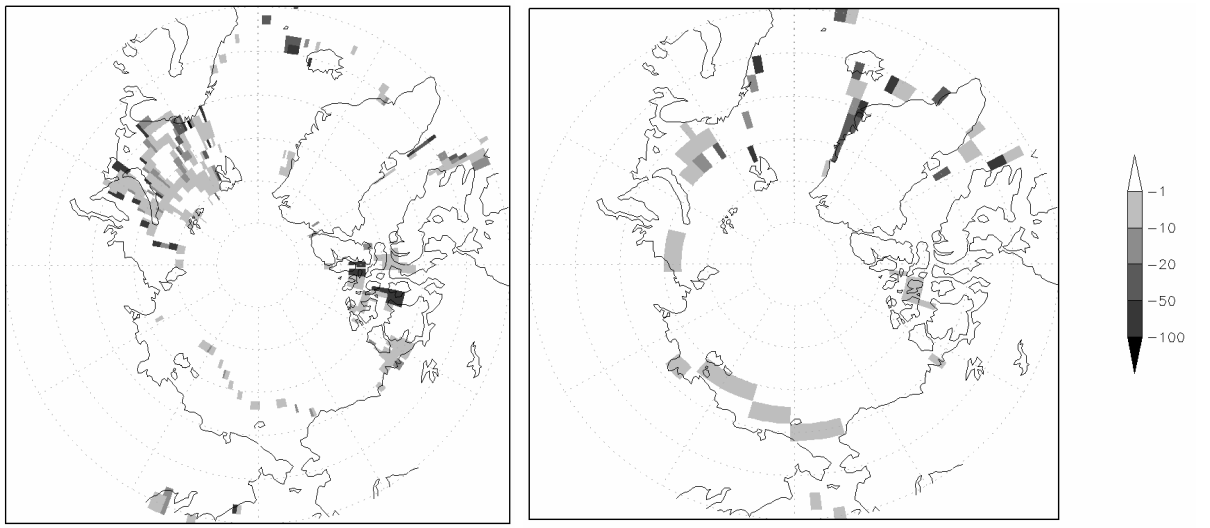

Fig 1. Changes in HSZ thickness (m) in the 21st century with GFDL (left) and INM (right) climate model forcing.

Response of the snow cover over France to climate change

Michel Déqué, Eric Martin and Nadia Kitova
Centre National de Recherches Météorologiques (CNRS/GAME), Météo-France.
42 avenue Coriolis F-31057 Toulouse Cédex 1, France, deque@meteo.fr

The climate change over the mountain regions is not an easy question because it is strongly modulated by the surface elevation and the horizontal gradient of this variable is not compatible with the horizontal resolution of the GCMs. The current resolution of the next CMIP5 exercise (100-200 km) does not allow to represent the mountains over France, except a coarse dome in the South-Eastern part corresponding to the Alps. The typical resolution of the next CORDEX exercise (50 km) enables to represent the main three mountains (Alps, Pyrenees and Massif Central) but the horizontal gradient of elevation is not steep enough and this has consequences on the representation of local precipitation and winds. In addition the maximum elevation is not high enough, which has consequences on the snow cover. Given the horizontal scale of ridges and valleys, a 1 km mesh would be necessary for an accurate representation of the mountains, but it is not yet compatible with centennial integrations with the present capacity of computers.

However the mid-latitude mountainous areas are vulnerable to global warming, because the reduction of the snow cover has a strong impact on water resources and tourism, even with a moderate increase in mean temperature. To investigate this question, we have developed, in the framework of the French national project SCAMPEI (http://www.cnrm.meteo.fr/scampei/) a four-step procedure to evaluate the snow cover over France:

Step one. The ARPEGE-climate-V4 AGCM model (Déqué, 2007) derived from the ARPEGE-IFS code has been run over 1950-2100 with monthly bias-corrected sea surface temperatures of the CMIP3 contribution by the AOGCM version of this model (A1B scenario). The AOGCM resolution is 300 km, whereas the AGCM has a variable horizontal resolution ranging from 50 km over Europe to 300 km in the southern Pacific.

Step two. The ALADIN-climate-V4 limited area RCM (Déqué and Somot, 2008) based on the above model, but with a 12 km resolution over a domain centered on France has been driven by the above AGCM. Figure 1 shows the surface elevation over France by the AOGCM, the AGCM, and the RCM.

Step three. The daily surface variables and fluxes have been corrected by the quantile-quantile method described in Déqué (2007). The reference data is the SAFRAN reanalysis (Quintana-Séguí et al., 2008). This reference offers hourly surface data and fluxes in 615 homogeneous areas within France (about 30 km horizontal resolution) at different altitudes (300 m vertical resolution).

Step four. The statistically corrected variables have been used as an input of the ISBA-ES soil-vegetation-snow model (Boone et al., 2001).

The output of this process is, inter alia, a daily data base of high resolution snow cover with different altitudes for each area. Because of the statistical pre-processing, the snow cover climatology is in fairly good agreement with the observations during the 1961-1990 period. The process has been repeated with SRES scenarios A2 and B1 in order to explore the uncertainty. It is planned to include two other French RCMs at similar resolution, and a direct statistical downscaling to SAFRAN data of some CMIP3 AOGCMs to deepen the uncertainty analysis.

Figure 2 shows the mean number of days per year with snow on the ground in France as a function of surface elevation for the 1961-1990 period (solid line), the 2021-2050 period (three dashed lines corresponding to B1, A1B and A2 forcings) and the 2071-2100 period (three dotted lines corresponding to B1, A1B and A2 forcings). One can see that up to 3000 m, the number of days with snow cover (> 1cm) decreases. The 3 mid-century scenarios have a similar response, whereas at the end of the century, the response is ranked by the GHG concentration. In the worse scenario (A2), The number of days with snow cover on the ground is reduced by 25% at 3000 m, 33% at 2400 m, 50% at 1800m and 75% at 1200m. This result confirms the sensitivity study in the Mont Blanc region by Martin et al. (1997).

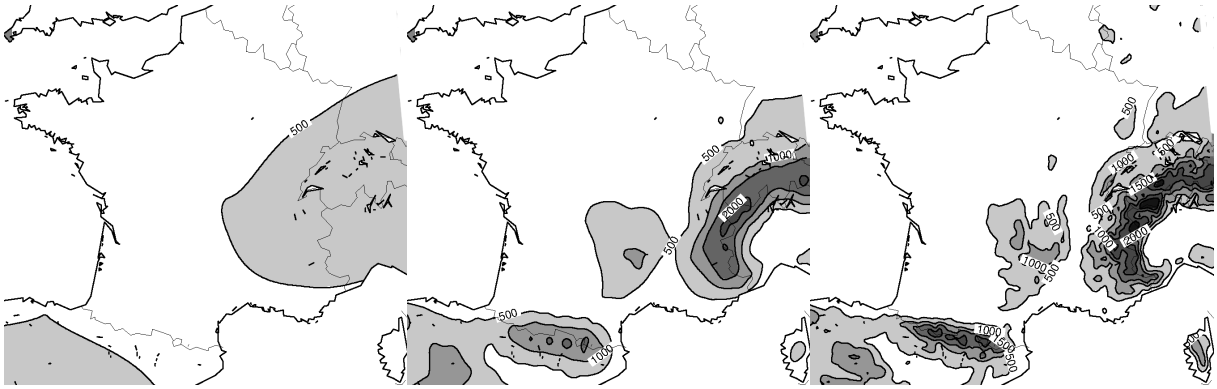

Figure 1: Surface elevation (m) of the 3 atmospheric models involved in the process. AOGCM (left, resol. 300 km), AGCM (middle, resol. 50 km), RCM (right, resol. 12 km). Contour interval 500 m

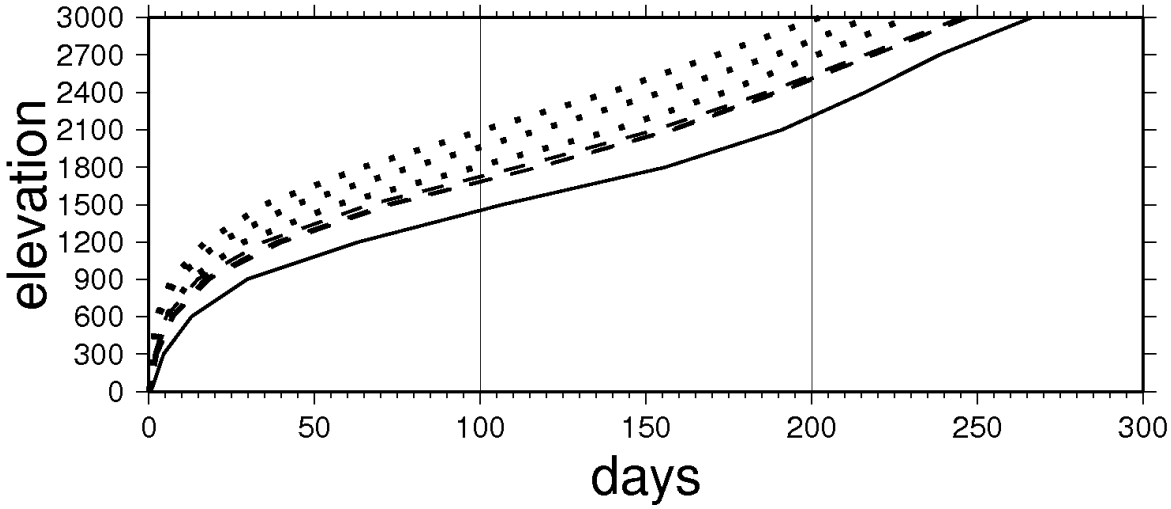

Figure 2: Mean number of days per year with snow on the ground (abscissa) as a function of surface elevation (ordinate, m) for 1961-1990 (solid), 2021-2050 (dash) and 2071-2100 (dot). The 3 scenarios correspond to B1, A1B and A2.

Acknowledgements:

This study was supported by the French national program ANR (VMCS08-SCAMPEI).

References:

Boone, A. and P. Etchevers, 2001: An inter-comparison of three snow schemes of varying complexity coupled to the same land-surface model: Local scale evaluation at an Alpine site, J.Hydrometeorol., 2, 374-394.

Déqué, M., 2007: Frequency of precipitation and temperature extremes over France in an anthropogenic scenario: model results and statistical correction according to observed values. Global and Planetary Change, 57, 16-26.

Déqué, M. and S. Somot, 2008: Extreme precipitation and high resolution with Aladin. Quarterly Journal of the Hungarian Meteorological Service, 112, 179-190.

Quintana-Seguí, P., P. Le Moigne, Y. Durand, E. Martin, F. Habets, M. Baillon, C. Canellas, L. Franchisteguy and S. Morel, 2008: Analysis of Near-Surface Atmospheric Variables: Validation of the SAFRAN Analysis over France. J. Appl. Meteor. Climatol., 47, 92–107.

Martin E., B. Timbal and E. Brun, 1997: Downscaling of general circulation model outputs: simulation of the snow climatology of the French Alps and sensitivity to climate change. Climate Dynamics, 13, 45-56.

Russian Heat Wave and Blockings Activity Changes

I.I. Mokhov, M.G. Akperov, A.A. Vetrova
A.M. Obukhov Institute of Atmospheric Physics RAS, Moscow, Russia
mokhov@ifaran.ru

The year 2010 was characterized by exceptional summer heat wave in the European part of Russia. This heat wave generated extensive forest and peat fires with extreme air pollution and vast societal impacts and economic damages. During two months with anomalously hot weather and highly polluted air the health risk was sharply increased (http://ifaran.ru/science/seminars/Summer2010.html).

The Russian heat wave in summer 2010 was triggered by long-term blocking situation in the Euro-Atlantic region. Frequency of atmospheric blockings in summer season is maximum near 30^{o}E over Eastern Europe. Estimates based on observations and model simulations (Lupo et al., 1997; Mokhov and Petukhov, 1997) display a tendency of increase of blockings duration under general warming. Additionally there is a tendency of decrease in precipitation accompanying the increase of temperature in spring-summer for midlatitudinal Eurasian regions, particularly for European part of Russia (Mokhov, 2005). Such tendencies promote to the increase of regional drought risk under global warming (Mokhov et al., 2005).

We analyzed possible changes of atmospheric blockings activity in the Northern Hemisphere (NH) in the 21st century from modern global model simulations. The analyzed projections are based on the CMIP3 ensemble of global climate model (GCM) simulations. In particular, simulations with the IPSL-CM4 GCM for 2001-2100 with SRES-A2 and SRES-A1B scenarios were used. Characteristics of the NH extratropical cyclonic/anticyclonic activity from simulations with this GCM were analyzed in (Mokhov et al., 2007; Mokhov et al., 2009) in comparison with characteristics based on reanalysis data. Similar analysis of extratropical anticyclonic/cyclonic activity was done for results of the INM RAS GCM simulations in (Akperov et al., 2007). Blocking characteristics were obtained from model simulations for 500-hPa heights with the use of different identification schemes, in particular with modified Lejenas-Okland criterion similar to (Wiedenmann et al., 2002) and by method based on scheme applied in (Akperov et al., 2007).

Analysis of possible changes in the extratropical cyclonic and anticyclonic activity displays large variability in the 21st century from different model simulations with anthropogenic forcing (Akperov et al., 2007; Mokhov et al., 2007; Mokhov et al., 2009). Quasistationary blocking anticyclones also display remarkable interannual and interdecadal variability. Figure 1 shows changes of the blocking-days number in summer for the NH Euro-Atlantic sector (60W-60E) by IPSL-CM4 GCM simulations from the second half of the 20th century to the end of the 21st century the with SRES-A2 scenario. These changes were detected with the use of modified Lejenas-Okland criterion.

According to Fig. 1 it can be expected the increase of the blocking-days number in summer for the NH Euro-Atlantic sector up to about 60 days. Such total duration of blocking situation was obtained from analyzed model simulations for summer 2012. This model estimate is close to real duration of blocking situation for European part of Russia in summer 2010. Besides the summer 2012 model simulations show 5 additional years (2018, 2022, 2037, 2043 and 2086) in the 21st century with the blocking-days number in summer larger than 50 days for the NH Euro-Atlantic sector.

This work was supported by RFBR, CRDF and RAS programs.

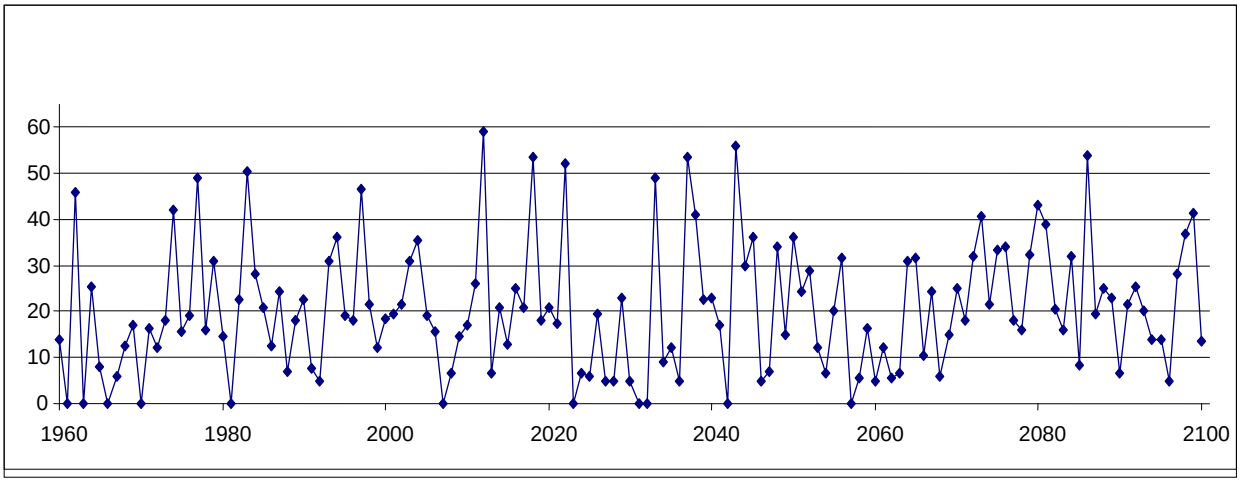

Figure 1. Variations of the blocking-days number in summer in the NH Euro-Atlantic sector (60W-60E) from model simulations with SRES-A2 scenario for the 21st century.

References

Akperov M.G., M.Yu. Bardin, E.M. Volodin, G.S. Golitsyn and I.I. Mokhov, 2007: Probability distributions for cyclones and anticyclones from the NCEP/NCAR reanalysis data and the INM RAS climate model. *Izvestiya, Atmos. Oceanic Phys.*, **43**, 705-712.

Lupo A.R., R.J. Oglesby and I.I. Mokhov, 1997: Climatological features of blocking anticyclones: A study of Northern Hemisphere CCM1 model blocking events in present-day and double CO_2 concentration atmospheres. *Climate Dyn.*, **13,** 181–195.

Mokhov I.I., 2005: Spring-summer climate extremes in Eurasian midlatitudinal regions. *Research Activities in Atmospheric and Oceanic Modelling,* J. Cote (ed.), WMO/TD-No.1276, Rep.35, 07.29-07.30.

Mokhov I.I., J.-L. Dufresne, H. Le Treut, V.A. Tikhonov and A.V. Chernokulsky, 2005: Changes in drought and bioproductivity regimes in terrestrial ecosystems of Northern Hemisphere by global climate model simulations with carbon cycle. *Doklady Earth Sci.*, **405A**(9), 1414-1418.

Mokhov I.I., M.G. Akperov, A.V. Chernokulsky, J.-L. Dufresne and H. Le Treut, 2007: Comparison of cloudiness and cyclonic activity changes over extratropical latitudes in Northern Hemisphere from model simulations and from satellite and reanalysis data. *Research Activities in Atmospheric and Oceanic Modelling,* J. Cote (ed.), WMO/TD-No.1397, Rep.37, 07.15-07.16.

Mokhov I.I., M.G. Akperov, J.-L. Dufresne and H. Le Treut, 2009: Cyclonic activity and its total action over extratropical latitudes in Northern Hemisphere from model simulations. *Research Activities in Atmospheric and Oceanic Modelling,* J. Cote (ed.), Rep.39, 07.9-07.10.

Mokhov I.I. and V.K. Petukhov, 1997: Blockings and their tendencies of change. *Doklady Earth Sci.*, **357**, 687-689.

Wiedenmann J.M., A.R. Lupo, I.I. Mokhov and E.A. Tikhonova, 2002: The climatology of blocking anticyclones for the Northern and Southern Hemispheres: Block intensity as a diagnostic. *J. Climate*, **15**(23), 3459–3473.

REGIONAL DYNAMICAL DOWNSCALING OF GISS-ER CLIMATE SIMULATIONS WITH FOCUS ON GULF OF MEXICO STATES

Georgy V. Mostovoy[1], Valentine G. Anantharaj[2], Yee H.Lau[3]

[1)]Geosystems Research Institute, Mississippi State University, Mississippi, USA (mostovoi@gri.msstate.edu)
[2)]National Center for Computational Sciences, Oak Ridge National Laboratory, Tennessee, USA
[3)]Northern Gulf Institute, Mississippi State University, Mississippi, USA

Dynamical downscaling is considered a generally reliable approach to extract more regional details from climate simulations performed with Global Climate Models (GCM). Recent studies (e.g. Liang et al. 2004, Lynn et al. 2010) show that, regional details in downscaled precipitation and air temperature fields are not noisy (despite the regional biases that may exist); and therefore might be valuable for assessing impacts of climate variability and change. In this study, the state-of-the-art Weather Research and Forecasting (WRF) model (Skamarock et al. 2006) was used as the regional climate model (RCM) to downscale global climate simulations over the southeastern United States, particularly in the northern Gulf of Mexico. WRF Version 3.2.1 was used to downscale the IPCC AR4 simulations from the NASA GISS-ER GCM (Russell et al. 2000, Schmidt et al. 2006). A set of two 11-year periods were used: 1990-2000 (20C3M scenario) and 2050-2060 (selected from the SRESA2 forcing scenario).

The following physical options were used: Kain-Fritsch cumulus parameterization; the WRF single-moment 5-class microphysics scheme; Rapid Radiative Transfer Model (RRTM) for longwave atmospheric radiation; the Goddard scheme for shortwave radiation; the Yonsei University parameterization for the atmospheric boundary layer; and the Noah land surface model with a 2-m deep soil layer. All the WRF-RCM simulations were performed at three nested domains with two-way coupling between the nests with grid spacing of 45-, 15-, and 5 km. The spatial extent of the inner fine-grid domain with 5 km grid spacing is shown in Fig. 1. The vertical levels in WRF were represented by 41 sigma-pressure levels. Initial and boundary data for were pre-processed from the GISS-ER model output (WCRP 2010). This conversion includes the modification of original atmospheric and land surface variables, their spatial interpolation from the GISS 4˚x5˚ latitude-longitude grid to 1˚x1˚ latitude-longitude grid, temporal interpolation, level/time subseting and units conversions. Missing values of air temperature, relative humidity, and wind components at low isobaric levels (1000 hPa, 925 hPa, and 850 hPa) were extrapolated from above.

Each of 11-years downscaling simulations were performed on a month-long basis (e.g. Lynn et al. 2010). Every month-long simulation was started from initial conditions retrieved from the GISS model data. To keep the WRF-based solution close to the GISS large-scale fields, a simple nudging approach was adopted above 700 hPa for the following model variables: air temperature, geopotential, water vapor mixing ratio, and wind components. The sea surface temperature (SST) was represented by the skin temperature field available from the GISS model output.

Three sets of mean 2 m air temperature fields averaged over the years 1990-2000 for the months of July and October are shown in Fig.1. The warmest overland temperatures are observed over the Mississippi Delta (having lower vegetation fraction in comparison with adjacent areas and therefore the higher surface temperature) and over the state of Louisiana. The spatial distribution of this warm bias indicates that it could be associated with a different specification of green vegetation fraction in the WRF-based RCM and in the NARR processing system/model. During July, the Mississippi Delta is clearly observed as a region of elevated surface air temperature both in RCM and in the NARR data, as shown in Fig. 1. Note that a better agreement between the NARR data and RCM simulations over the Delta is due to fine spatial resolution (5 km grid spacing) used in the RCM. During January, the GISS model produces a marked cold bias of about 3 ˚C in the northern part of the domain. In April, the surface air temperature is consistently warmer in the RCM simulations if compared with the corresponding NARR data over the 5 km domain (not shown). Fig. 2 illustrates the mean annual cycle (averaged for 1990-2000) of the surface (at 2 m level above the ground) air temperature. In general, the RCM-downscaled simulations show a closer agreement with the NARR data as compared with the output from the GISS model, except for spring and the northern part of the 5 km domain. Typically, the GISS model shows lower values of surface temperature having negative monthly mean bias of 2-3 ˚C, as compared to temperatures from the NARR data and RCM simulations. Figure 3 shows mean annual cycles (averaged for 1990-2000 and for 2050-2060) of the surface air temperature simulated with the WRF-based

RCM. An overall increase of monthly mean temperatures (a warming trend of the surface air temperature) between 1990-2000 and 2050-2060 is quite clear in Fig. 3. Both the RCM simulations and the GISS model indicate the most substantial increase of surface air temperature, exceeding 3 °C during February, September, and October (see left frames in Fig. 3). Finally, the RCM and the GISS model failed to reproduce a correct annual precipitation cycle, especially over northern part of the 5 km domain. Contrary to the NARR data, these two models produced an excessive increase in precipitation amount from April to August.

REFERENCES

Liang, X-Z, Li Li, K.E. Kunkel, M. Ting, and J. X.L. Wang, 2004: Regional climate model simulation of U.S. precipitation during 1982-2002. Part I: Annual cycle. *J. Climate*, **17**, 3510-3529.

Lynn, B.H., and Coauthors, 2010: Testing GISS-MM5 physics configurations for use in regional impact studies. *Clim. Change*, **99**, 567-587.

Russell, G.L., J.R. Miller, D. Rind, R.A. Ruedy, G.A. Schmidt, and S. Sheth. 2000: Comparison of model and observed regional temperature changes during the past 40 years. *J. Geophys. Res.*, **105**, 14891-14898.

Schmidt, G.A., and Coauthors, 2006: Present-day atmospheric simulations using GISS ModelE: Comparison to in situ, satellite, and reanalysis data. *J. Climate*, **19**, 153-192.

Skamarock, W.C., J.B. Klemp, J. Dudhia, D.O Grell, D.O. Gill, D.M. Barker, W. Wang, and J.G. Powers, 2006: A description of the advanced research WRF. *NCAR Technical Note*, NCAR/TD-468+STR, 88pp.

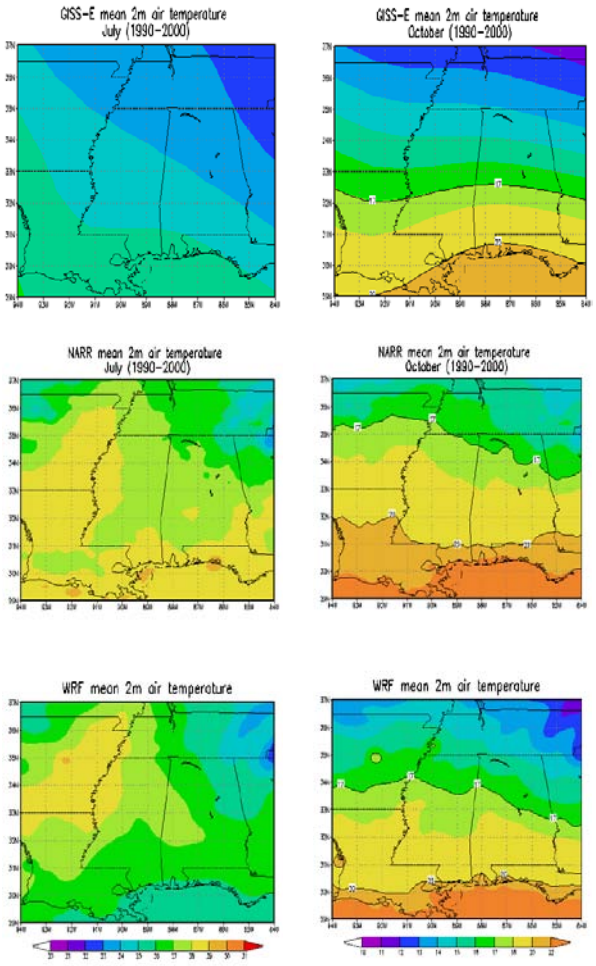

Figure 1. Distribution of air temperature at 2m for July (left frames) and October (right) from NARR data (middle frames) and from GISS-E model (upper frames) and WRF-based downscaling (lower frames) averaged for 11 years (1990-2000).

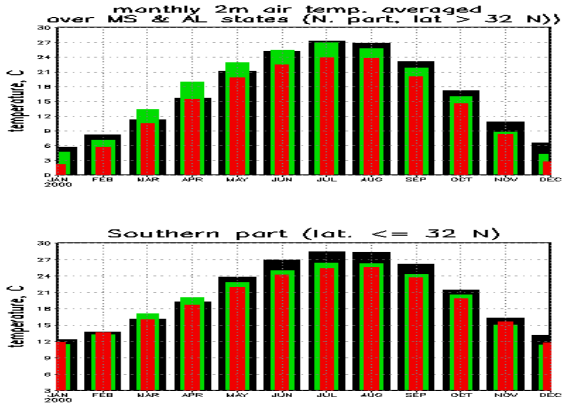

Figure 2. Comparisons of monthly mean 2 m air temperature (averaged for 5-km domain) between NARR data (black bars) and WRF-based RCM (green) for 1990-2000. Red bars stands for temperature from GISS model. Northern part of the domain (upper frame) and southern part (lower).

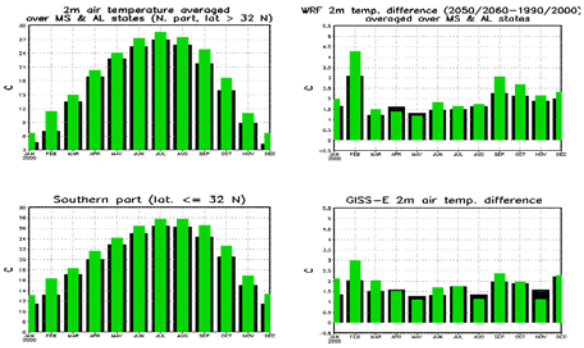

Figure 3. Monthly mean 2 m air temperature (left frames) for 1990-2000 (black bars) and 2050-2060 (green) and their difference (right frames) from WRF-based RCM simulations. Right frames: black bars indicate northern part of the domain and green – southern part.